Annular Josephson tunnel junctions in an external magnetic field: The statics

N. Martucciello
Dipartimento di Fisica, Università di Salerno, I-84081, Baronissi (SA), Italy

R. Monaco
Dipartimento di Fisica, Università di Salerno, I-84081, Baronissi (SA), Italy
and Istituto di Cibernetica del C.N.R, I-80072, Arco Felice (NA), Italy
(Received 27 June 1995; revised manuscript received 28 September 1995)

We have investigated the static configurations of the phase inside an annular Josephson tunnel junction in the presence of an externally applied magnetic field. We report here a detailed study of the dependence on the magnetic field of the critical current for different annular geometries. The periodic conditions for the phase difference across the barrier are derived from fluxoid quantization. For rings having a radius less than the Josephson penetration depth analytical results are derived which are in excellent agreement with the experimental data. For longer junctions numerical analysis is carried out after the derivation of the appropriate perturbed sine-Gordon equation. We find that a number of different phase profiles may exist for a given applied field which differ according to the number of fluxon-antifluxon pairs present in the line. Experimental data support the theoretical analysis provided self-field effects are taken into account in real devices.

I. INTRODUCTION

A Josephson tunnel junction is certainly one of the most convenient solid-state device for the study of the nonlinear phenomena and, in particular, long Josephson tunnel junctions, i.e., junctions for which at least one dimension is greater than the Josephson penetration depth, are useful for the investigation of the soliton properties. Most of the experimental work has been carried out on linear quasi-one-dimensional junctions having either the overlap geometry in which the bias current flows perpendicular to the long dimension or the inline geometry in which the bias current flows parallel to the long dimension. Very little work has dealt with annular, i.e., ring-shaped junctions even though, they offer many advantages for the study of the soliton dynamics. The situation is slightly different with regard to numerical investigations of long Josephson tunnel junctions. In fact, papers have often dealt with both linear and annular geometries and, in some cases, only the annular geometry was considered. It was recognized a long time ago that soliton (or fluxon) motion is smoother in ring-shaped junctions since the fluxon cannot collide with boundaries.[1] Another unique property of annular junctions results from fluxoid quantization in a superconducting ring: one or more fluxons can be trapped in the junction at the time of the normal-superconducting transition. Once trapped the fluxons can never disappear and only fluxon-antifluxon pairs can be nucleated. Dueholm *et al.*[2] reported experimental results on fluxon motion in long annular junctions. Later on, a number of people found this geometry ideal for experimental tests of the perturbation models developed to take into account the dissipative effects in the pure sine-Gordon analysis.[3–5] The dynamics of the single and multiple fluxons was also studied with the help of a low-temperature scanning electron microscope and in barriers with periodic inhomogeneities.[6–8] Recently the presence of vortices trapped in discrete Josephson rings has attracted the interest of the scientific community.[9,10] However, a detailed study of the behavior of annular junctions has never been undertaken and a full understanding of the possible new phenomena is far from complete. In particular, the behavior of an annular junction in the presence of an externally applied field has not previously been considered, to our knowledge.

In this article we focus our attention on the static configuration of the phase in ring-shaped junctions in the presence of an external applied field. The dynamics of solitons in annular junctions in the presence of an externally applied field will be the subject of another article. We have measured the dependence of the zero-voltage Josephson current for a large number of annular junctions having different geometries and normalized lengths. The experimental data are compared with the analytical results for small rings and with the numerical results obtained by solving the appropriate partial differential equations for large rings.

The paper is organized as follows. In Sec. II we describe the fabrication of the samples and the different geometries that have been realized; the proper periodic conditions are derived for each geometrical configuration. In Sec. III we present experimental data and the analytical results for an electrically short annular junction. In Sec. IV we derive the appropriate partial differential equation for a electrically long junction considering proper boundary conditions. In Sec. V we present the results of the numerical simulations and we demonstrate the existence of more than one phase profile for a given field. In Sec. VI we present some magnetic patterns for long annular junctions together with interpretation and discussion of the measurements. Conclusions are drawn in Sec. VII.

II. THE SAMPLES

Using the well known and reliable selective niobium anodization process[11] we have fabricated a large number of square and annular junctions based on the Nb/Al-AlO_x/Nb

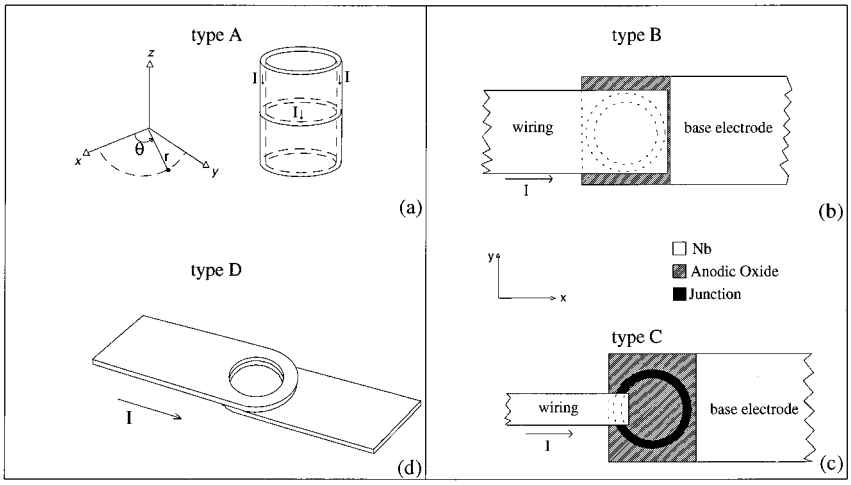

FIG. 1. Schematic of (a) type-*A*, (b) type-*B* and (c) type-*C* annular junctions considered in this work. Ideal type-*A* devices were used only as a simple example for theoretical purposes. (d) Geometrical configuration (type *D*) examined in previous reports.

technology. Small square junctions were used to measure the electrical properties of the Nb/Al-AlO_x/Nb trilayer. The details of the trilayer deposition and of the fabrication process can be found elsewhere.[12] On each substrate four identical annular junctions were made having an average circumference $C=500$ μm corresponding to a mean radius $\bar{r}=80$ μm and ring width $\Delta r=30$ μm. In this section we describe the different geometrical configurations that were considered. They are depicted in Figs. 1(a)–1(d). In Fig. 1(a) we show the perspective view of an ideal annular junction made by two semi-infinite hollow cylinders separated by a thin dielectric film; this configuration will be examined only theoretically. We will refer to this geometry as type-*A* geometry. Figure 1(b) shows the type-*B* geometry in which the annulus is sandwiched between two thick simply connected superconducting layers. Niobium anodic oxide (200 nm thick) and, sometimes, an extra dielectric layer made of rf-sputtered silicon dioxide (150 nm thick) provide a good insulation between the base electrode and the wiring film around the junction area. This thick insulating layer inside and outside the ring, also called idle region, is expected to alter both the static and dynamic properties of the junctions. However, on linear one-dimensional long junctions it has been proved by both numerical simulation[13] and experiments[12] that, as far as the static properties are concerned, the only effect of the idle region is to increase the magnetic energy stored in the fluxons, i.e., it introduces a scaling factor on the field strength. The schematic of type-*C* geometry is shown in Fig. 1(c): it is very similar to type *B* with the difference that the wiring film does not cover the entire junction top electrode but contacts it only in a very limited area. This difference, in principle, allows magnetic field to be trapped in the superconducting ring made by the junction top electrode at the time of the phase transition. We have realized only annular junctions of types *B* and *C* and often type-*B* junctions were obtained from type-*C* junctions after the deposition of an extra wiring film. In Fig. 1(d) we also show a geometrical configuration which has been used in previous experimental works aimed to the study of the fluxon propagation in the absence of boundary collisions.[4,5] This geometry, which will be referred to as type *D*, is such that magnetic flux can be trapped in the two superconducting rings, i.e., the base and top electrodes are both multiply connected superconductors.

In general, the periodic conditions for the quantum-mechanical phase difference ϕ across the barrier around an annular junction are written as

$$\phi(X+C)=\phi(X)+2\pi n, \tag{2.1}$$

$$\phi_x(X+C)=\phi_x(X), \tag{2.2}$$

where X is the spatial coordinate specifying the distance around the ring, C is the average ring circumference and n is an integer number corresponding to the algebraic sum of fluxons trapped in the junction at the time of the normal-to-superconducting transition. Equations (2.1) and (2.2) are physically reasonable since they state that observable quantities such as the Josephson current (through $\sin\phi$) and the magnetic field (through ϕ_x) must be single valued upon a round trip. We will give a derivation of Eq. (2.1) and will show that the number of trapped fluxons also depends on the particular geometry of the annular junction.

Let us start by considering fluxoid quantization applied to the type-*D* geometry. By choosing two closed and parallel paths in the top and base electrodes just above and just below the barrier we can write

$$\frac{m}{n_s e^2}\int_u \mathbf{J}_{su}\cdot d\mathbf{l}+\int_S\int_u \mathbf{B}\cdot d\mathbf{S}=k\Phi_0,$$

$$\frac{m}{n_s e^2}\int_l \mathbf{J}_{sl}\cdot d\mathbf{l}+\int_S\int_l \mathbf{B}\cdot d\mathbf{S}=j\Phi_0,$$

for the upper and lower paths, respectively. $\mathbf{J}_{su}$ and $\mathbf{J}_{sl}$ are the supercurrent densities in the upper and lower electrodes, respectively. $\Phi_0=h/2e$ is the flux quantum, while k and j indicate the integer numbers of flux quanta (in general, different) corresponding to each fluxoid. Taking the difference between the last two equations, and, considering that the two surface integrals must be equal, we end up with

$$\frac{m}{n_s e^2}\left(\int_u \mathbf{J}_{su}\cdot d\mathbf{l}-\int_l \mathbf{J}_{sl}\cdot d\mathbf{l}\right)=n\Phi_0 \tag{2.3}$$

with $n=k-j$. After some lengthy but straightforward calculations, we obtain the following equation:

$$\frac{m}{n_s e^2}(\mathbf{J}_{su}-\mathbf{J}_{sl})\cdot d\mathbf{l}=\phi_x dl,$$

which, inserted in Eq. (2.3), yields Eq. (2.1), for the devices having the type-*D* geometry. In other words, the net number of fluxons trapped in a annular junction comes out to be the algebraic difference between the number of fluxons associated with the fluxoids in each electrode. In the case of type-*D* geometry we have considered closed curves which surround a nonsuperconducting region, i.e., a hole. Magnetic flux can thread this hole accompanied by a current flowing round the hole. The fluxoid enclosed within each curve will be an integral number of flux quanta, but this number will be zero if no flux threads the hole. If, however, we consider a closed curve which does not encircle a nonsuperconducting region, so that the area enclosed by the curve is entirely superconducting, then the number of flux quanta is always zero. In other words, if we apply the fluxoid quantization to the type-*B* annular junctions, we must put $k=j=0$ in Eqs. (2.3) and (2.4), that is,

$$\phi(X+C)=\phi(X). \tag{2.4}$$

The last equation states that only fluxon-antifluxon pairs, and not isolated fluxons, can be trapped in a type-*B* annular junction passing through the normal-to-superconducting transition in presence of a magnetic field. This can be easily understood considering that, if a magnetic-field line enters the barrier in some place to create, e.g., a fluxon, it must necessarily exit at some other point in the barrier where it creates an antifluxon: in other words, a static fluxon-antifluxon pair has been created. When the field is removed and a bias current is supplied to the junction, the fluxon and the antifluxon start to move toward one another and the pair annihilates. This behavior has been experimentally proven on our type-*B* devices: in fact, we never succeeded in trapping an isolated fluxon in the barrier even after repeated thermal cycles through the transition temperature in the presence of an external field. We always found the same value for the zero-field critical current. The presence of one or more fluxons alone would cause a strong reduction, in principle, a total suppression, of the zero-voltage Josephson current as has been observed on type-*D* devices.[4] For type-*C* devices, from a theoretical point of view, we would expect the more general periodic condition [Eq. (2.1)] to hold, however, also in this case we were not able to trap flux in the barrier. Although surprising, this result is very similar to those reported by Davidson, Dueholm, and Pedersen on type-*D* devices realized on a superconducting ground plane;[4] in type-*C* devices the base electrode itself acts as a ground plane. At the moment it is not clear the role played by the ground plane on the periodic phase conditions.

III. SMALL ANNULAR JUNCTION

In this section we derive the equations which describe the behavior of a small annular junctions in the presence of a uniform external applied magnetic field. We will use cylindrical coordinates r, θ, and z, assuming that the junction lies in the $z=0$ plane and its center of symmetry is located at $r=0$, as shown in Fig. 1. We set the origin of the angular abscissa, i.e., $\theta=0$ in the direction of the field. The tunnel currents flow in the z direction and the local density of the Josephson current can be expressed as[14]

$$J_j(r,\theta)=J_c(r,\theta)\sin\,\phi(r,\theta), \tag{3.1}$$

where the maximum Josephson current density J_c, generally speaking, depends on both r and θ and is constant inside uniform barrier junctions. In Josephson's description the two-dimensional field ϕ is related to the voltage V across the two superconducting films and to the induction field $\mathbf{H}$ inside the barrier[14]

$$\frac{d\phi}{dt}=\frac{2\pi}{\Phi_0}V,$$

$$\nabla\phi=\frac{2\pi d\mu_0}{\Phi_0}\mathbf{H}\times\mathbf{u}_z, \tag{3.2}$$

in which $\mathbf{u}_z$ is a unit vector in the z direction, μ_0 is the vacuum permeability, and d is the junction magnetic penetration depth ($d=s+\lambda_{L1}+\lambda_{L2}$ where s is the thickness of the junction barrier and λ_{L1} and λ_{L2} are the London penetration depths of the superconducting electrodes). Equation (3.2) states that, among other things, ϕ is not sensitive to fields along the z direction.

We assume that the annular junction is electrically short, i.e., the ring circumference is small with respect to the Josephson penetration length λ_j. Further, by denoting with r_e and r_i the outer and inner ring radius, respectively, we assume that the ring width $\Delta r=r_e-r_i$ is much smaller than the mean radius $\bar{r}=0.5(r_e+r_i)$. Under these conditions a spatially homogeneous applied field H^* fully penetrates the barrier. This implies that the magnetic field is the same on both inside and outside of the ring, which is true only for the type-*C* geometry. Now, assuming $\phi=\phi(\theta)$, and considering that, according to Eq. (3.2), the dependence of ϕ on θ is related only to the radial component of the field $H_r=H^*\cos\,\theta$, integrating we get

$$\phi(\theta)=\eta\,\sin\,\theta+\phi_0, \tag{3.3}$$

where η is the externally applied field H^* normalized to $\Phi_0/2\pi\mu_0\bar{r}d$ and ϕ_0 is an integration constant. In other words, a small annular junction behaves as a small linear junction in a spatially modulated external field. The Josephson current through the barrier is obtained integrating Eq. (3.1) over the junction area. Assuming that the maximum Josephson current density J_c is constant over the junction area, we obtain for the total current,

$$I=\int J_j dS=J_c\bar{r}\Delta r\int_{-\pi}^{\pi}\sin\,\phi(\theta)d\theta. \tag{3.4}$$

Inserting Eq. (3.3) in Eq. (3.4) and carrying out simple calculations we get

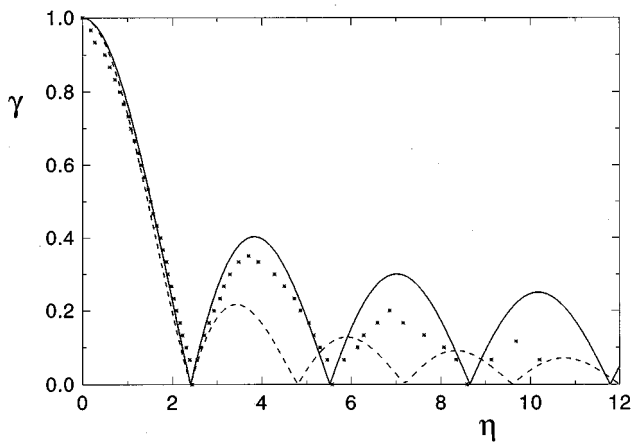

FIG. 2. Magnetic pattern of a small annular junction. The solid line represent the theory while the stars are the experimental data for a type-*C* junction having $C=1.7\lambda_j$. The dashed line shows for comparison the Fraunhofer-like theoretical dependence for a small rectangular junction. Field values have been normalized in such a way that the first minima coincide.

$$I(\eta,\phi_0)=I_c(0)\sin\ \phi_0\ \frac{1}{2\pi}\int_{-\pi}^{\pi}\cos(\eta\ \sin\ \theta)d\theta$$

$$=I_c(0)\sin\ \phi_0 J_0(\eta),$$

in which $I_c(0)=J_c 2\pi\bar{r}\Delta r$ is the maximum junction critical current and J_0 is the zero-order Bessel function. I is largest when $\phi_0=\pi/2$ so[15]

$$I_c(\eta)=\max_{\phi_0} I(\eta,\phi_0)=I_c(0)|J_0(\eta)|.$$

The theoretical magnetic-field dependence of the normalized critical current $\gamma(\eta)=I_c(\eta)/I_c(0)$ of a small annular junction is shown by the full curve in Fig. 2. The first zero of J_0 occurs for $\eta_c=2.405$. For comparison we also show the Fraunhofer dependence typical of small linear junctions $|\sin(\eta\pi/\eta_c)/(\eta\pi/\eta_c)|$ (dashed line in Fig. 2). It is evident that for an annular junction in a uniform field the minima in the magnetic pattern are not integer multiples of the first one, although they are (almost) equally spaced, the separation between two contiguous minima being about π. The second zero occurs for $\eta_2=5.52=2.29\eta_c=\eta_c+3.12$, the third occurs for $\eta_3=8.65=3.60\eta_c=\eta_2+3.13$ and, for larger arguments the minima can be found using the approximate relation $J_0(\eta)\simeq\sqrt{2/\pi\eta}\cos(\eta-\pi/4)$. Further, the secondary maxima in the Bessel pattern are more pronounced than those of the Fraunhofer pattern. The experimental data for an annular junction with the type-*C* geometry and average circumference $C=1.7\lambda_j$ are reported by stars in Fig. 2. The field scale for the experimental data has been chosen in such a way that the first minimum in the pattern coincides with the first minimum of $J_0(\eta)$. It is evident that the experimental data nicely reproduce the main features of the Bessel pattern, although discrepancies in the amplitudes of the secondary maxima show up especially for large field values. [For the sake of completeness, a comparison of the $J_0(\eta)$ dependence found for small annular junctions with the $J_1(\eta)/0.5\eta$ dependence known for small circular junctions[16] shows that in the latter case the secondary minima occurs at η values which are lower than the integer multiples of η_c, that is, $\eta_2=1.83\eta_c$, $\eta_3=2.65\eta_c$, and so on.] We wish to comment that, if the applied field is not uniform but is radial, as that generated by a current circulating in a loop concentric with the ring as in Ref. 6, each section of the ring feels the same field and the annular junction follows a Fraunhofer-like magnetic pattern.

So far we have assumed a uniform Josephson current density J_c, however the analysis can be generalized to the cases in which J_c has a simple dependence on θ. We have limited our interest to sinusoidally modulated current distributions such as

$$J_c(\theta)=J_{c0}\ \frac{1+a\ \cos\ n(\theta-\theta_0)}{1+a},\tag{3.5}$$

where is a is a positive constant less than one, θ_0 is a generic angle, n is a positive integer and $J_{c0}=J_c(\theta_0)$ is one of the maxima of the critical current density. Inserting Eq. (3.5) in Eq. (3.4), we obtain the result of the integration in terms of higher-order Bessel functions:

$$I_c(\eta)=\frac{I_c(0)}{1+a}\ \sqrt{J_0^2(\eta)+a^2\ \sin^2\ \theta_0 J_n^2(\eta)},$$

for odd n. Instead, if n is even, we get

$$I_c(\eta)=\frac{I_c(0)}{1+a}\ |J_0^2(\eta)+a^2\ \sin^2\ \theta_0 J_n^2(\eta)|.$$

Equation (3.5) can be generalized to describe any periodic distribution expanded in a Fourier series as, for example, those realized on annular junctions with periodic dishomogeneities proposed by Ustinov.[17]

IV. LONG ANNULAR JUNCTIONS: THE THEORY

In this section we derive the appropriate sine-Gordon equation for an annular junction in an external magnetic field. The total tunnel current density is given by

$$J_z=J_c\ \sin\ \phi+\frac{\Phi_0}{2\pi R}\ \phi_t,$$

where the second term in the right side takes into account the quasiparticle tunnel current assumed to be Ohmic, i.e., R is the voltage-independent quasiparticle resistance per unit area. The subscripts on ϕ denote partial derivatives. By combining the previous equations with Maxwell's equations, one obtains a differential equation for ϕ:

$$\lambda_j^2\nabla^2\phi-\frac{1}{\omega_p^2}\ \phi_{tt}-\sin\ \phi=\frac{\phi_t}{\omega_p^2 R c_s}-\lambda_j^2\epsilon_r\epsilon_0 R_s\nabla^2\phi_t,$$

where $\lambda_j^2=\Phi_0/2\pi\mu_0 J_c d$ and $\omega_p^2=2\pi J_c/\Phi_0 c_s$, c_s being the specific junction capacitance. It is well known that the parameter λ_j, called the penetration length of the junction, gives a measure of the distance over which significant spatial variations of the phase occur, in the time-independent configuration. The plasma frequency $\omega_p/2\pi$ represents the oscillation frequency of small amplitude waves. Further, we can introduce the parameter $\bar{c}=\omega_p\lambda_j$ which gives the velocity of light in the barrier and is called Swihart velocity. In the last

equation the second term in the right side takes into account the effect of the surface currents in the London layers, i.e., R_s is the voltage-independent surface resistance. Introducing the adimensional loss coefficients $\alpha^{-1}=\omega_p R c_s$ and $\beta=\epsilon_r\epsilon_0\omega_p R_s$, the last equation takes the form:

$$\lambda_j^2\nabla^2\phi-\frac{1}{\omega_p^2}\,\phi_{tt}-\sin\,\phi=\frac{\alpha}{\omega_p}\,\phi_t-\lambda_j^2\beta\nabla^2\phi_t. \quad (4.1)$$

Equation (4.1) is called perturbed sine-Gordon equation (PSGE). Because of its local form, it is quite general and holds for junctions of any geometrical configuration. It becomes more familiar in normalized Cartesian coordinates[1]

$$\phi_{xx}+\phi_{yy}-\phi_{tt}-\sin\,\phi=\alpha\phi_t-\beta(\phi_{xxt}+\phi_{yyt}).$$

On the junction boundary the continuity of the induction field is such that, according to Eq. (3.2),[18]

$$\nabla\phi=\kappa\mathbf{H}^{\rm ext}\times\mathbf{u}_z,$$

with $\kappa=2\pi d\mu_0/\Phi_0$. $\mathbf{H}^{\rm ext}$ is the external field that, in general, is given by the sum of an externally applied field and the field generated by the current flowing in the junction. The last vectorial equation can be split into its components:

$$\frac{\partial\phi}{\partial r}=\kappa H_\theta^{\rm ext}\quad\text{and}\quad\frac{1}{r}\,\frac{\partial\phi}{\partial\theta}=\kappa H_r^{\rm ext}. \quad (4.2)$$

The exact knowledge of the radial and tangential components of the external field allows the determination of the proper boundary conditions. Now we recall that the Laplacian of ϕ in cylindrical coordinates is expressed as

$$\nabla^2\phi=\frac{1}{r}\,\frac{\partial\phi}{\partial r}+\frac{\partial^2\phi}{\partial r^2}+\frac{1}{r^2}\,\frac{\partial^2\phi}{\partial\theta^2}. \quad (4.3)$$

Equations (4.1) and (4.3) are, generally speaking, the starting point for the study of junctions having circular symmetry. However, the exact junction geometry must be taken in consideration. As a first case and as a simple example, we consider an ideal annular junction made by two semi-infinite thick-walled hollow superconducting cylinders as shown in Fig. 1(a). A bias current I_b flowing uniformly and parallel to the cylinder axis generates, according to Ampere's law, a tangential field $I_b/2\pi r$ at a distance r from the axis (only outside the cylinder), the self-field being zero inside the cavity. Further, assuming that the cylinder walls are much thicker than the London penetration depth λ_L, i.e., that the ring width $\Delta r\gg\lambda_L$, an external and uniform field H^* applied parallel to the barrier plane (as said before, at $z=0$), will be shielded inside the cavity because of the demagnetization currents flowing on the external surface of the cylinders. (We assume here that the applied field is not strong enough to drive the superconductors into the intermediate state.) It is well known that the screening currents modify the configuration of the external field and, by using the fact that the field component parallel to a surface is continuous across it, it comes out that the tangential field is given $H_t=H^*/(1-N)=2H^*$ where N is the demagnetizing geometrical factor which is equal to 0.5 for a cylinder immersed in a field normal to its axis. The direction of this field is such that it adds to the self-field on one side and subtracts on the other. Therefore, considering that the junction boundaries are at $r=r_i$ and $r=r_e$, the boundary conditions Eqs. (4.2) for this geometry can be written as

$$\left.\frac{\partial\phi}{\partial r}\right|_{r=r_i}=0$$

and

$$\left.\frac{\partial\phi}{\partial r}\right|_{r=r_e}=-\kappa(2H^*\,\sin\,\theta+I_b/2\pi r_e). \quad (4.4)$$

If the ring width $\Delta r=r_e-r_i$ is smaller than λ_j, we can assume that $\partial\phi/\partial r$ varies linearly between r_e and r_i to give

$$\frac{\partial\phi}{\partial r}=-\kappa(2H^*\,\sin\,\theta+I_b/2\pi r_e)\,\frac{r-r_i}{\Delta r} \quad (4.5)$$

and, differentiating with respect to r

$$\frac{\partial^2\phi}{\partial r^2}=-\frac{\kappa}{\Delta r}\,(2H^*\,\sin\,\theta+I_b/2\pi r_e). \quad (4.6)$$

Substituting Eqs. (4.5) and (4.6) into Eq. (4.3) and eliminating the dependence on r by introducing the mean radius $\bar r=(r_e+r_i)/2=r_e-\Delta r/2$, Eq. (4.1) can be written as

$$\left(\frac{\lambda_j}{\bar r}\right)^2\phi_{\theta\theta}-\frac{1}{\omega_p^2}\,\phi_{tt}-\sin\,\phi=\gamma+\eta\Delta\,\sin\,\theta+\frac{\alpha}{\omega_p}\,\phi_t-\left(\frac{\lambda_j}{\bar r}\right)^2\beta\phi_{\theta\theta t},$$

where $\gamma=I_b/J_c 2\pi\bar r\Delta r=I_b/I_c(0)$ represents the distributed bias current normalized to the maximum Josephson critical current, η, as in Sec. III, is the externally applied field H^* normalized to $\Phi_0/2\pi\mu_0 d\bar r$ and $l=C/\lambda_j$ is the normalized ring mean circumference. Defining the dimensionless wave number $k=2\pi/l$, the quantity $\Delta=k^2(1+2\bar r/\Delta r)$ is a geometrical factor which sometimes has been referred to as the coupling between the external field and the flux density of the junction.[19] In passing, we note that the smaller the width Δr, the more sensitive is the junction to an external field. However, in the limit of vanishing small Δr, Eqs. (4.4) cannot be satisfied simultaneously, and some penetration of the external field inside the cavity must be allowed. Finally, introducing the new dimensionless angular coordinate $x=\bar r\theta/\lambda_j$ and normalizing the time to ω_p^{-1}, we obtain the perturbed Sine-Gordon equation (PSGE), for an annular Josephson tunnel junction of type A:

$$\phi_{xx}-\phi_{tt}-\sin\,\phi=\gamma+\eta\Delta\,\sin\,kx+\alpha\phi_t-\beta\phi_{xxt},$$

with the periodic conditions given by Eqs. (2.1) and (2.2).

We now consider the more realistic type-B and type-C geometries depicted in Fig. 1(b) and Fig. 1(c), respectively, in which the annular junctions are realized by means of planar films. In these cases the screening currents can be neglected and the boundary conditions Eqs. (4.2) can be written as

$$\left.\frac{\partial\phi}{\partial r}\right|_{r=r_i}=0$$

and

$$\left.\frac{\partial\phi}{\partial r}\right|_{r=r_e} = -\kappa(H^* \sin\theta + I_b/2\pi r_e)$$

for the geometrical configuration of Fig. 1(b), and

$$\left.\frac{\partial\phi}{\partial r}\right|_{r=r_i} = -\kappa H^* \sin\theta$$

and

$$\left.\frac{\partial\phi}{\partial r}\right|_{r=r_e} = -\kappa(H^* \sin\theta + I_b/2\pi r_e),$$

for the geometrical configuration of Fig. 1(c). Carrying out the calculations, one ends up with the following differential equation for $\phi(x,t)$:

$$\phi_{xx} - \phi_{tt} - \sin\phi = \gamma + \eta\Delta \sin kx + \alpha\phi_t - \beta\phi_{xxt}, \qquad (4.7)$$

in which $\Delta = k^2(1/2 + \bar{r}/\Delta r)$ in the case of Fig. 1(b) and $\Delta = k^2$ in the case of Fig. 1(c). Equation (4.7) states that for an annular junction the magnetic field enters directly into the PSGE in contrast to the case of linear junctions for which it appears only in the boundary conditions. Further, the different sections of the ring *feel* different field; more precisely, diametrically opposed points *feel* opposite field and the field term in Eq. (4.7) is in phase with respect to the actual field. Moreover, as before, the effect of a given field is larger on small width rings, but only for the type-*B* geometry. In the case of type-*C* geometry the behavior is independent on both $\bar{r}$ and Δr, however, the coupling factor Δ is always smaller than that of the type-*B* geometry, i.e., type-*C* devices are less sensitive to the external field. In all cases, the effect of a given field decreases quadratically with the ring normalized circumference l. At first glance one may think that Eq. (4.7) is the PSGE for an overlap junction in a spatially modulated magnetic field or with a spatially modulated bias term, however, closer consideration shows that this is not the case.

In what follows, since we are interested in the static, i.e., time-independent solutions of Eq. (4.7), we will focus our attention on the following equation:

$$\phi_{xx} - \sin\phi = \gamma + \eta\Delta \sin kx, \qquad (4.8)$$

and, in order to fix the number of solitons in the junction to zero, the condition on the phase periodicity is given by

$$\phi(x+l) = \phi(x), \qquad (4.9)$$

$$\phi_x(x+l) = \phi_x(x). \qquad (4.10)$$

Setting $\gamma = \eta = 0$, Eq. (4.8) is a well-known equation which describes the phase distribution in a linear in-line-type junction with the proper boundary conditions set by the bias current and the external field. Ferrel and Prange[20] found for a semi-infinite linear junction a solution which satisfies the boundary condition, $\phi(\infty) = 0$. Later, in a famous paper by Owen and Scalapino,[21] Eq. (4.8) was analytically solved (for a finite in-line junction) in terms of Jacobian elliptic functions and the vortex structures have been carefully studied. It was shown that, for a given field and bias, different phase distributions $\phi(x)$ are allowed which differ according to the number of static fluxons in the barrier. This also explains the multiple solutions found in the measurements of the magnetic dependence of the critical current of long linear junctions.[16,22] (The case $\gamma \neq 0$ and $\eta = 0$ which describes long overlap junctions in external field cannot be solved analytically, but has been analyzed by Pagano, Ruggerio, and Sarnelli in phase space[23] since the equation can be integrated once to give $\phi_x = \pm\sqrt{2(K' - \cos\phi - \gamma\phi)}$, where K' is an integration constant. Unfortunately, the presence of the η term does not allow a similar analytical treatment.)

V. LONG ANNULAR JUNCTIONS: THE NUMERICAL SIMULATIONS

We have numerically solved Eq. (4.8) for different values of the normalized circumference l which enters the equation directly through k and Δ. Direct numerical integration of Eq. (4.8) is complicated by instabilities associated with the absence of damping in the system.[24] To avoid this problem, we reverted to the integration of Eq. (4.7) with $\alpha = 1$, in order to obtain convergence to a static solution through a rapid decay of transient. In real device $\alpha \leqslant 0.01$. The term containing the surface losses was simply dropped to save computer time, i.e., $\beta = 0$. Equation (4.7) was integrated using an implicit finite difference method.[25] The integration in time is given by a standard fourth-order Runge-Kutta algorithm and the integration in space by the usual three-point approximation for the second derivative.

We have numerically computed the maximum allowed

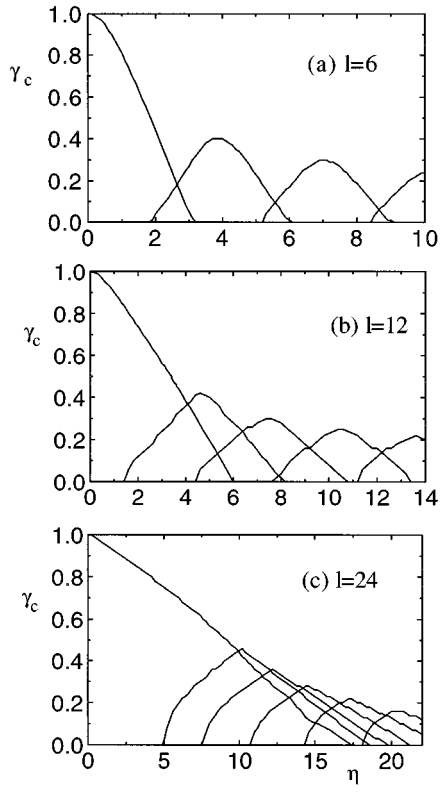

FIG. 3. Numerically computed threshold curves of long annular junctions having different normalized circumferences l. (a) $l = 6$, (b) $l = 12$, and (c) $l = 24$.

value of the zero-voltage bias γ_c vs η for annular junctions having different normalized circumferences l. In these simulations, l had to be an integer number. We have carried out the calculations for junctions having the type-C geometry, i.e., with $\Delta=k^2$, however, if type-A or type-B geometries are considered the proper value for Δ has to be inserted in Eq. (4.8). For $l=1$, the numerical data closely follow the expected Bessel-like dependence $\gamma_c=|J_0(\eta)|$ with differences only in the third significant digit. Pronounced deviations from the theoretical behavior of small junctions were found for $l=6$, as can be seen in Fig. 3(a) where the γ_c vs η dependence is reported. In fact, for large l we find ranges of magnetic field, near minima of the threshold curve, in which γ_c may assume two different values. In a fashion which closely recalls the behavior of long linear junctions, these values correspond to different configurations of the phase inside the barrier. In fact, each lobe in Fig. 3(a) is associated with a given vortex structure; more precisely, in the first lobe which extends from $\eta=0$ to $\eta=\eta_c=3.2$, the external magnetic field is shielded and no vortices penetrate the barrier. However, at the very end of this lobe a full fluxon-antifluxon pair is present along the junction, the fluxon facing the antifluxon on diametrically opposed potential wells created by the magnetic field. The different phase profiles will be analyzed in detail later. In the successive lobes the magnetic field penetrates in the barrier and vortices enter the barrier in a way analogous to the behavior of the type-II superconductors, even though the junction vortices differ from the Abrikosov vortices in that they lack a normal core. In the second lobe, extending from $\eta=1.8$ to $\eta=6.1$, we begin with a phase configuration very similar to that at the right side of the first lobe in which one fluxon-antifluxon pair is present in the barrier, and we end with two fluxon-antifluxon pairs, the two bunched fluxons facing the two bunched antifluxons in diametrically opposed potential wells created by the magnetic field. Adopting the terminology used for the linear junctions,[21] we refer to the first lobe as the ''0 to 1 (fluxon-antifluxon) pair mode'' lobe, the second as the ''1 to 2 pair mode'' lobe and so on. In general, one may talk about the n to $n+1$ pair mode when the junction contains more than n pairs, but less than $n+1$ pairs. As l is increased, η_c increases, each lobe broadens, and, sometime, three or more lobes overlap. This behavior is shown in Fig. 3(b) for an annular junction with $l=12$ where up to five lobes are plotted. $\eta_c=6.0$ for this normalized length. In order to trace the different lobes, it is crucial to start the integration with the proper initial phase profile. Initially the phase configurations corresponding to zero, one, two, etc. fluxon-antifluxon pairs were found on a short junction ($l=3$) for which the lobe overlap is very small. Later these profiles were scaled and used as approximate initial configurations for longer junctions ($l=6,12,24$). However, on real devices, the measurements of maximum supercurrent against the external field often yield the only envelope of the lobes, i.e., the current distribution switches automatically to the mode which for a given field carries the largest supercurrent. Sometimes, for a given applied field, multiple solutions are observed on a statistical basis by sweeping the junction current-voltage characteristic many

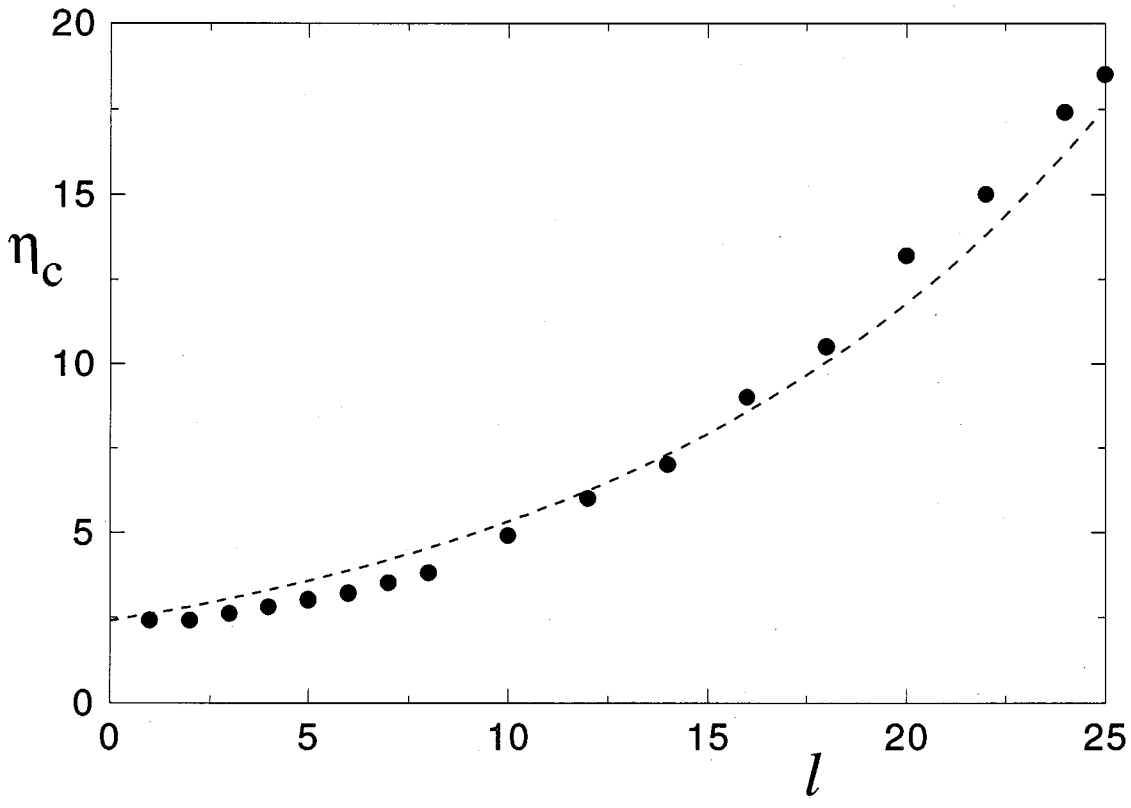

FIG. 4. Dependence of the critical field η_c on the normalized circumferences of the ring l. Dots denote numerically computed data and the solid line is an empirically found relationship.

times. Increasing l further, the dependence of the first lobe becomes more and more linear and its slope becomes less and less pronounced. For $l=24$ the critical field is 18.6, as shown in Fig. 3(c).

The numerically computed critical field values found on junctions with different lengths are plotted as dots in Fig. 4 together with an empirical but simple exponential law (solid line) which nicely fits the numerical data,

$$\eta_c = \eta_c(0)\exp\frac{l}{4\pi}.$$

We do not have arguments to give physical support to this relationship.

Going back to Fig. 3(c), we observe that for $l=24$, there exists a range of values of η from 14.5 to 17.4 for which five different vortex configurations are possible. For $\gamma=0.05$ and $\eta=15$, these configurations are shown in Figs. 5 where the Josephson current density profile $\sin\phi(x)$ (solid line) and the local magnetic field $\phi_x(x)$ (dashed line) are reported simultaneously. In the 0 to 1 pair mode [Fig. 5(a)] almost one fluxon-antifluxon pair is uniformly distributed along the barrier and the magnetic field in the junction is very weak since we are still in the Meissner region where the external fields tend to be shielded. As we move toward the 4 to 5 pair mode [Fig. 5(e)], we observe that $\sin\phi(x)$ makes more and more oscillations between $+1$ and -1 and the magnetic field grows larger. Each $\sin\phi$ oscillation corresponds to a $\pm 2\pi$ phase change, i.e., to a fluxon or antifluxon depending on the sign of ϕ_x. We can clearly see that the fluxons (antifluxons) are bunched together and they tend to accumulate where the external field is tangent to the ring and its effect is weaker, that is at $x=\pm l/4$. These points correspond to a minimum of a potential and the fluxons (antifluxons) are in a stable equilibrium. When the number of fluxons in a potential well increases, their widths and the distance between them decreases, despite the repulsive force experienced by two or more closely spaced fluxons, seen as magnetic dipoles. In second approximation, we may also consider the attractive forces between one or more fluxons at, say, $x=+l/4$ and one or more antifluxons at $x=-l/4$; in fact, since they are at diametrically opposed points of the ring their magnetic dipoles line up. For each of the configurations shown in Figs. 5, as we increase the external field, a further torque is applied along the line; however, the torque has opposite polarity on opposite sides and is maximum at the points $x=0$ and $x=l/2$, where the fluxon-antifluxon pairs are nucleated.

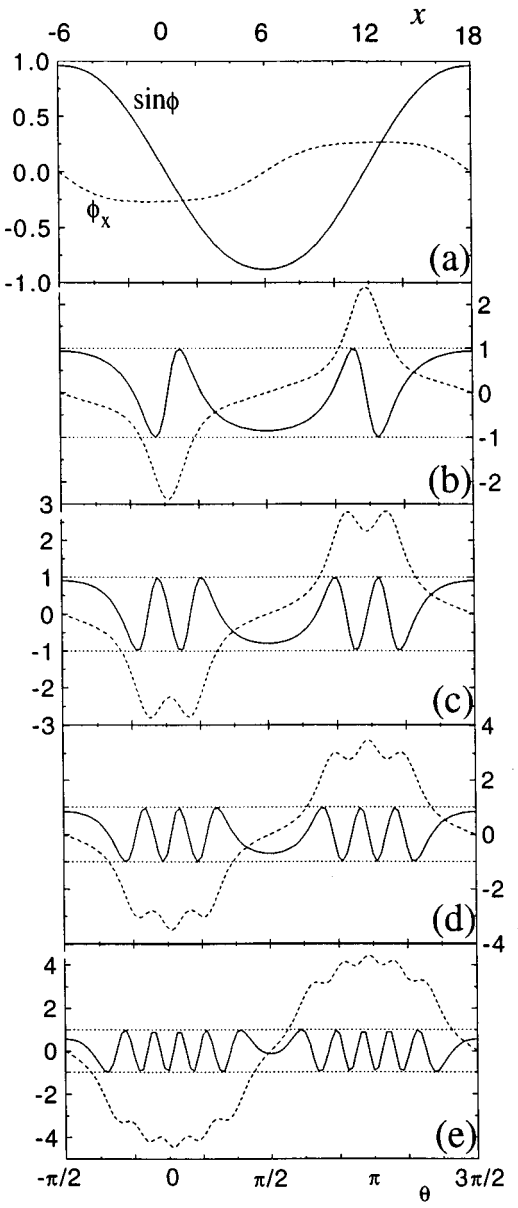

FIG. 5. The spatial dependence of the current density $\sin\phi$ (solid line) and the local magnetic field ϕ_x (dashed line) for an annular junction of length $l=24$. (a), (b), (c), (d), and (e) represent the five vortex structures for $\eta=15$ and $\gamma=0.05$.

VI. LONG ANNULAR JUNCTIONS: THE MEASUREMENTS

In this section we present some representative magnetic threshold patterns of annular junctions for various geometries, normalized lengths and orientations of the externally applied field. We begin with the two patterns shown in Fig. 6; they refer to the same junction measured in the type-C (dashed line) and in the type-B (solid line) configurations. In fact, as said before, a number of samples were first fabricated in the type-C configuration and, after the measurement at liquid-helium temperature, the deposition of an extra and larger wiring film was deposited to obtain the type-B geometry. The quasiparticle I-V characteristics of the samples measured in these two configurations were very similar indicating that the superconducting properties of the junction top electrode (50 nm thick) are not affected by the presence of a thick backing Nb film. In order to avoid self-field effects the maximum Josephson current density of this sample was measured on a small square junction belonging to the same fabrication batch. We found $J_c=15$ A/cm^2, which yields $\lambda_j=110$ μm and $l\simeq 5$; further, we measured a ratio of the maximum Josephson current to the current jump at the gap voltage $I_c/\Delta I_g=0.55$ (due to the proximity effect, such a small value is typical of symmetric low-current-density Nb/Al-AlO$_x$-Al/Nb junctions).

The maximum critical currents occur for zero applied field; however, the zero-field Josephson current for the type-B device is larger (about twice) than that measured in

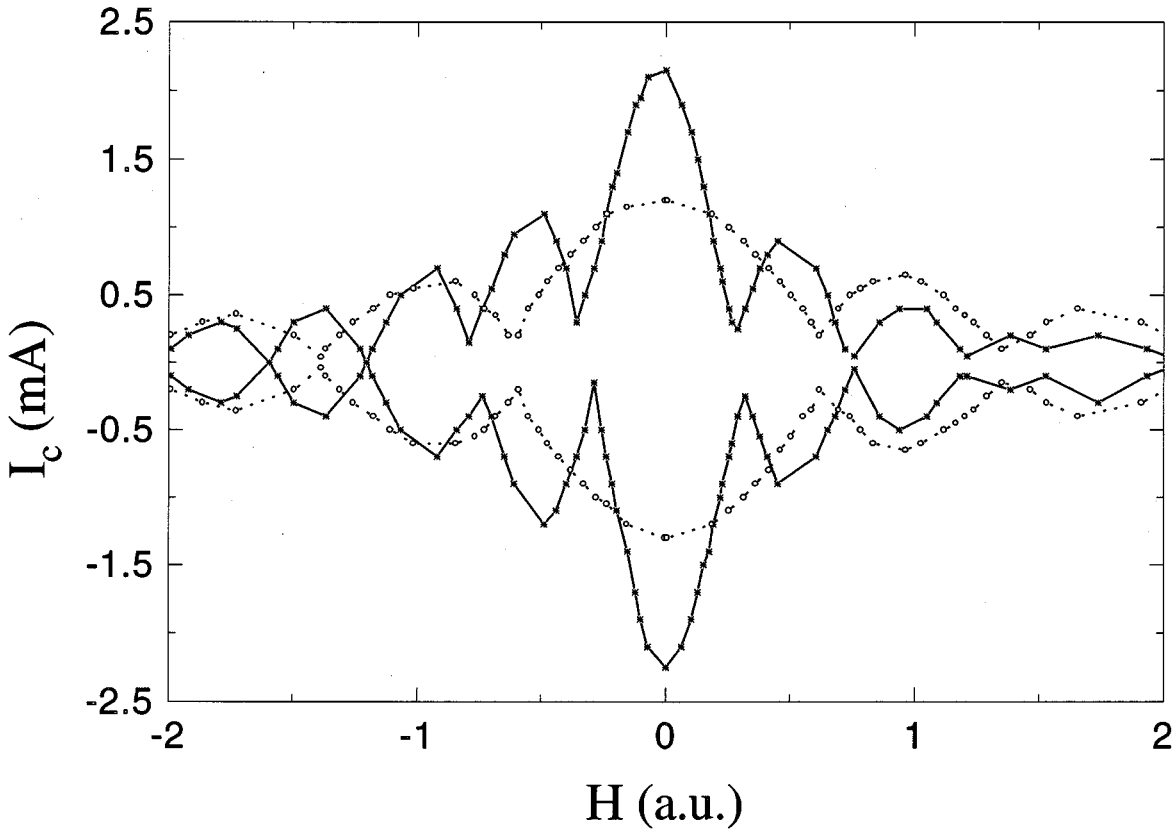

FIG. 6. Magnetic pattern of a intermediate-length annular junction in the type-*B* (solid line) and in the type-*C* (dashed line) configuration.

the type-*C* configuration. This effect closely recalls of linear junctions in the in-line and overlap configurations and suggests that, in type-*C* geometry, the bias current is not uniformly distributed over the junction area. The ratio $I_c/\Delta I_g$ is a direct measure of this nonuniformity: the lower this ratio, the larger is the nonuniformity. For the the type-*B* geometry this ratio is slightly less than that found on a small square junction so that we can assume that the bias current is distributed uniformly. However, the value measured in the type-*C* configuration (0.28) indicates that the bias current mainly enters the junction near $\theta=0$.

Another evident feature in Fig. 6 is that the minima of the two patterns do not occur for the same value of the external field (although the field strength on the abscissa is reported in arbitrary units, these units are the same for the two sets of data). The ratio of the critical field measured in the type-*B* configuration to the critical field obtained in the type-*C* configuration is 0.55; in Sec. IV we have observed that the type-*B* samples are expected to be more sensitive to the external field, however, according to the calculated coupling factors Δ, we would expect this ratio to be $1/(1/2+\bar{r}/\Delta r)=0.33$. This discrepancy can be accounted for, at least qualitatively, by the presence of the idle region inside the type-*B* devices. It has been shown for linear junctions that the lateral idle region increases the fluxon rest mass[13] and, in turn, the junction critical field.[12] Indeed, we always find some discrepancy between the experimental and theoretical coupling factors. In particular, the coupling between the external field and the flux density in the junction was found to depend on the width of the base electrode and on the location of the annular junction on the base electrode itself. These facts indicate that, from a theoretical point of view, other geometrical factors must be taken into account to compute the exact value of Δ. For this reason all the experimental I_c vs H dependences reported in these paper use arbitrary units for the field.

The reduced zero-field critical current of type-*C* devices indicates that these samples experience a field due the bias current itself. Since the bias current flows mainly in the *x* direction [see Fig. 1(c)], the self-field occurs principally in the *y* direction. To better understand the nature of the self-

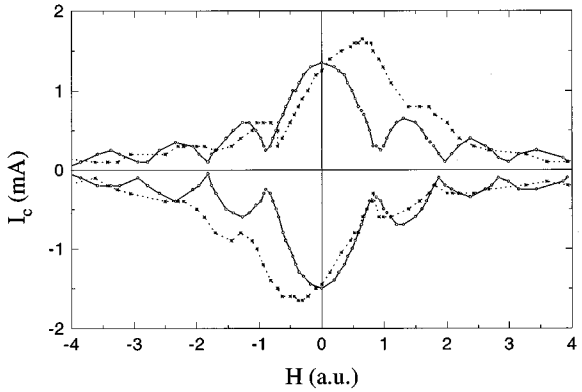

FIG. 7. Magnetic pattern of a type-*C* intermediate-length annular junction with different orientation of the external field. Parallel to the bias current (solid line), i.e., *x* direction in Figs. 1(b) and 1(c), and perpendicular to the bias current (dashed line), i.e., *y* direction in Figs. 1(b) and 1(c).

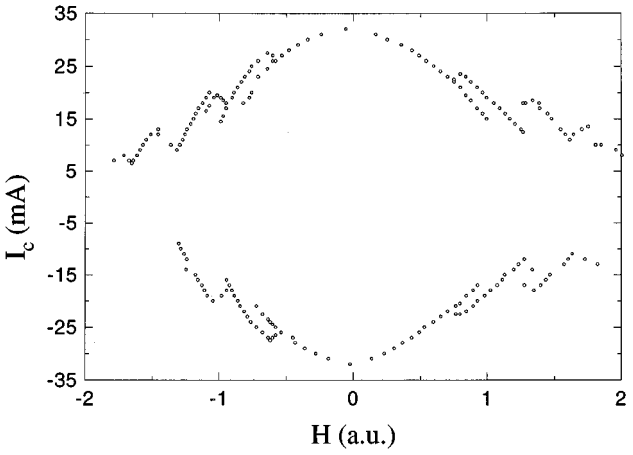

FIG. 8. Magnetic pattern of a long ($l=17$) annular junction in the type-*B* configuration.

field, we have compared the magnetic patterns of one (type-*C* geometry) annular junction taken with the orientation of the external magnetic field in the *x* direction and in the *y* direction. The results of these measurements are shown in Fig. 7 for a sample having $J_c=15$ A/cm^2 and $l\simeq 5$. The solid line shows the data for the field in the *x* direction, while the dashed line corresponds to data taken with the field in the *y* direction. We observe that, while in former case the pattern is symmetric with respect to the inversion of the current and/or the field, in the latter the dependence shows the typical behavior of linear junctions immersed in an external field parallel to their own self-field;[26] in fact, the largest value of the critical current occurs for a field which is comparable with the critical field measured with the field parallel to the bias current. Furthermore, the ratio of the maximum critical current to the current rise at the gap voltage is very close to that measured on a small square junction, so that we can reasonably assume that the self-fields are almost completely compensated by a field perpendicular to the current flow. This hypothesis is supported by the result of numerical integration of Eq. (4.8) with an extra term which simulates a uniform self-field parallel $\rho\gamma\Delta\sin kx$ and orthogonal $\rho\gamma\Delta\cos kx$ to the external field applied in the *x* direction (i.e., parallel to the bias current flow). A behavior very close to that shown in Fig. 7 has been simulated by setting the free parameter $\rho=2$.

We have shown numerical [cf. Fig. 3(a)] and experimental (cf. Fig. 6) evidence that, when the junction circumference is less than about $2\pi\lambda_j$ the effects of static self-field, although evident, are not very pronounced. To conclude this section, we show in Fig. 8 the magnetic pattern of a long (type-*B*) annular junction with $J_c=210$ A/cm^2 and $l=\simeq 17$. For small fields, the dependence is not quite linear as expected for long junctions, however, the occurrence of multiple solutions clearly indicates the existence of different vortex states. However, for this sample the ratio $I_{c,\max}/\Delta I_g I_{c,\max}/\Delta I_g=(32$ mA)/(67 mA)$=0.48$. The same sample measured with the field in the *y* direction had a maximum critical current of 42 mA, while a similar junction in the type-*C* configuration had a maximum critical current of 19 mA in nonzero field. These facts suggest that current limiting effects due to the self-fields also play an important role for long junctions in the type-*B* geometrical configuration and this consideration should apply also to devices having the type-*D* geometry. We also speculate that the quadratic dependence for small fields can be attributed to self-field effects.

VII. CONCLUSIONS

The dependence of the critical current on a uniform magnetic field for annular Josephson tunnel junctions has been investigated both experimentally and numerically. A simple analytical approach is possible when the normalized ring circumference is less than $\simeq 2\pi$. In this case we find that I_c vs H does not follow the Fraunhofer-like pattern typical of rectangular junctions, but rather a zero-order Bessel function behavior, with almost equally spaced minima. Different junction geometries have been considered in studying the static self-field in long annular junctions. However, two planar structures characterized by a simply connected base electrode have been chosen for the experiments. We saw no evidence of fluxon trapping when the samples were cooled in an external field. For each geometry we have derived a partial differential equation to describe both the statics and the dynamics of the phase difference across the barrier. When static solutions were numerically computed, we found that, for a given field, different phase profiles are possible depending on the number of fluxon-antifluxon pairs nucleated at two diametrically opposed points in the barrier where the effect of the field is largest. Experimental data on high-quality Nb/Al-AlO_x-Al/Nb annular junctions basically confirm the theoretical predictions provided the effects of current limiting static self-field are taken into account.

ACKNOWLEDGMENTS

The authors wish to thank Professor R. D. Parmentier and Dr. S. Pagano for stimulating discussions and for a critical reading of the manuscript; further we acknowledge A. Ferrentino for a valuable technical assistance. This work was partially supported by the Consiglio Nazionale delle Ricerche under the Progetto Finalizzato ''Superconductive and Cryogenic Technologies.''

[1] D. W. McLaughlin and A. C. Scott, Phys. Rev. A **18**, 1652 (1978).

[2] B. Dueholm, A. Davidson, C. C. Tsuei, M. J. Brady, K. H. Brown, A. C. Callegari, M. M. Chen, J. H. Greiner, H. C. Jones, K. K. Kim, A. W. Kleinsasser, H. A. Notarys, G. Proto, R. H. Wang, and T. Yogi, in *Proceedings of LT-17*, edited by U. Eckerm, A. Schmid, W. Weber, and H. Wuhl (Elsevier, Amsterdam, 1984).

[3] A. Davidson, B. Dueholm, B. Kryger, and N. F. Pedersen, Phys. Rev. Lett. **55**, 2059 (1985).

[4] A. Davidson, B. Dueholm, and N. F. Pedersen, J. Appl. Phys. **60**, 1447 (1986).

[5] A. V. Ustinov, T. Doderer, R. P. Huebener, N. F. Pedersen, B. Mayer, and V. A. Oboznov, Phys. Rev. Lett. **69**, 1815 (1992).

[6] A. V. Ustinov, T. Doderer, B. Mayer, R. P. Huebener, I. V. Vernik, and V. A. Oboznov, in *Proceedings of SQUID '92*, edited by H. Koch and H. Lubbig (Springer-Verlag, Berlin, 1992).
[7] I. V. Vernik, V. A. Oboznov, and A. V. Ustinov, Phys. Lett. A **168**, 319 (1992).
[8] A. Laub *et al.* (unpublished).
[9] A. V. Ustinov, M. Cirillo, and B. A. Malomed, Phys. Rev. B **47**, 8357 (1993).
[10] H. S. J. van der Zant, T. P. Orlando, S. Watanabe, and S. H. Strogatz, Phys. Rev. Lett. **74**, 174 (1994).
[11] H. Kroger, L. N. Smith, and D. W. Jillie, Appl. Phys. Lett. **39**, 280 (1981).
[12] R. Monaco, G. Costabile, and N. Martucciello, J. Appl. Phys. **77**, 2073 (1995).
[13] J. G. Caputo, N. Flytzanis, and M. Devoret, Phys. Rev. B **50**, 6471 (1994).
[14] B. D. Josephson, Phys. Lett. **1**, 251 (1962).
[15] A. Barone and G. Paternò, *Physics and Applications of the Josephson Effect* (Wiley, New York, 1982).
[16] J. Matisoo, J. Appl. Phys. **40**, 1813 (1969).
[17] A. V. Ustinov, Phys. Lett. A **136**, 155 (1989).
[18] S. Pagano, Ph.D. thesis, Technical University of Denmark, 1987.
[19] N. Grönbech-Jensen, P. S. Lomdahl, and M. R. Samuelsen, Phys. Lett. A **154**, 14 (1991).
[20] R. A. Ferrel and R. E. Prange, Phys. Rev. Lett. **10**, 479 (1963).
[21] C. S. Owen and D. J. Scalapino, Phys. Rev. **164**, 538 (1967).
[22] K. Schwidtal, Phys. Rev. B **2**, 2526 (1970).
[23] S. Pagano, B. Ruggiero, and E. Sarnelli, Phys. Rev. B **43**, 5364 (1991).
[24] We observe that, in Eq. (4.8) if the time t replaces the spatial coordinate x and a new phase $\phi' = \phi - \pi$ is defined, we end up with the equation which describes the motion of a simple lossless pendulum with a constant applied torque γ plus a harmonic forcing term with amplitude $\gamma_{ac} = \eta\Delta$ at a angular frequency $\Omega = k$, when normalized to the pendulum natural frequency ω_p: $\phi'_{tt} + \sin\phi' = \gamma + \gamma_{ac}\sin\Omega t$. The periodic condition Eq. (4.9), in terms of the period $T = 2\pi/\Omega$ becomes $\phi(t+T) = \phi(t)$ and implies that after one rf cycle the phase must assume the same value. Now, since we are dealing with a conservative system, the power $\phi_t(\gamma + \gamma_{ac}\sin\Omega t)$ must average to zero over one rf cycle, giving $\phi_t(t) = \Sigma A_n \cos n\Omega t$; in other words, ϕ_t must be an even function. Further, ϕ_t must be periodic: $\phi_t(t + 2\pi/\Omega) = \phi_t(t)$, i.e., in the average the phase derivative is zero. In terms of the small Josephson junction driven by a dc and rf current, it means that the system has to remain on the zero-voltage state. It is straightforward to establish that the static solution for an annular junction with n trapped fluxons is analogous to that of a lossless rf-driven point junction on the nth rf induced step.
[25] S. Pagano (private communication).
[26] T. Yamashita and Y. Onodera, J. Appl. Phys. **38**, 3523 (1976).